Improved Ground Hydrology Calculations for Global Climate Models (GCMs): Soil Water Movement and Evapotranspiration

F. ABRAMOPOULOS

CENTEL Sigma Data Services, Corp., NASA/Goddard Space Flight Center, Institute for Space Studies, New York

C. ROSENZWEIG

Department of Geography, Columbia University and NASA/Goddard Space Flight Center, Institute for Space Studies

B. CHOUDHURY

NASA/Goddard Space Flight Center, Greenbelt, Maryland

(Manuscript received 9 July 1987, in final form 6 April 1988)

ABSTRACT

A physically based ground hydrology model is developed to improve the land–surface sensible and latent heat calculations in global climate models (GCMs). The processes of transpiration, evaporation from intercepted precipitation and dew, evaporation from bare soil, infiltration, soil water flow, and runoff are explicitly included in the model. The amount of detail in the hydrologic calculations is restricted to a level appropriate for use in a GCM, but each of the aforementioned processes is modeled on the basis of the underlying physical principles. Data from the Goddard Institute for Space Studies (GISS) GCM are used as inputs for off-line tests of the ground hydrology model in four 8° × 10° regions (Brazil, Sahel, Sahara, and India). Soil and vegetation input parameters are calculated as area-weighted means over the 8° × 10° gridbox. This compositing procedure is tested by comparing resulting hydrological quantities to ground hydrology model calculations performed on the 1° × 1° cells which comprise the 8° × 10° gridbox. Results show that the compositing procedure works well except in the Sahel where lower soil water levels and a heterogeneous land surface produce more variability in hydrological quantities, indicating that a resolution better than 8° × 10° is needed for that region. Modeled annual and diurnal hydrological cycles compare well with observations for Brazil, where real world data are available. The sensitivity of the ground hydrology model to several of its input parameters was tested; it was found to be most sensitive to the fraction of land covered by vegetation and least sensitive to the soil hydraulic conductivity and matric potential.

1. Background

Atmospheric scientists have used simple parameterizations for evaporation from land surfaces in global climate models (GCMs). These parameterizations have been reviewed by Carson (1982). In general, the schemes make two crude assumptions in order to simplify the complexity of the evaporation processes over land: 1) a soil moisture availability function based on simple water budget and field capacity accounting is used in place of a physically modeled soil hydrology; and 2) evaporation is modeled without explicit physiological resistance from vegetation. This approach does not allow the role of vegetation in the hydrologic cycle to be portrayed realistically nor does it permit detailed study of biosphere–climate interactions.

Utilizing theoretical advances from plant physiology, micrometeorology and hydrology, several GCM research groups are currently engaged in model improvement in order to parameterize more realistically the exchange of fluxes between the atmosphere and the biosphere. Dickinson (1984) described a parameterization for a detailed calculation of evapotranspiration which includes soil water movement, vegetation storage and evaporation of intercepted precipitation and dew, and the partitioning of vegetational surface area into transpiring (leaves) and nontranspiring (stems) segments. Sellers et al. (1986) have also developed a parameterization of land–surface atmosphere processes which includes the interaction of vegetation with radiation, vertical water movement in the soil, conduction of soil water through the vegetation layer, interaction of photosynthetically active radiation with integrated stomatal functioning of the canopy, evapotranspiration, and rainfall interception and evaporation.

These more detailed evapotranspiration parameterizations, however, are dependent on adequate descrip-

Corresponding author address: Dr. Frank Abramopoulos, CENTEL Sigma Data Services Corp., Goddard Institute for Space Studies, 2880 Broadway, New York, NY 10025.

tions of the highly variable physical and biological characteristics of the land surface. It is unknown how detailed this characterization of soil and vegetation must be in order to model realistically climate with a GCM. Sensitivity tests with the improved evapotranspiration models both off-line and linked to the GCMs should help to determine climate sensitivity to the surface parameters and therefore the optimum level of detail for describing land–surface characteristics and processes to be included in the GCMs.

Our primary objective is to provide a more realistic yet still simple calculation of evaporation from land surfaces for GCMs by including realistic soil water flow, explicit vegetative resistance, evaporation from intercepted precipitation and dew, evaporation from bare soil, and the partition of soil water loss due to transpiration according to root density. A schematic representation of the processes included in the ground hydrology model is shown in Fig. 1. Other objectives are to test the use of composite vegetative and soil characteristics developed from small-scale observations in the evapotranspiration calculations at gridbox 8° lat × 10° long (or 4° lat × 5° long) resolutions and to test the model's sensitivity to soil and vegetation characteristics.

a. Comparison with simpler model

The ground hydrology model has been designed as a candidate for incorporation into the Goddard Institute for Space Studies (GISS) GCM (model II as described in Hansen et al. 1983). It represents an improvement over that used in the GISS GCM in the following respects:

1) Multiple soil layers may be used instead of two in order to provide a more realistic description of soil water dynamics.
2) Realistic hydraulic conductivity and matric potential functions are specified rather than a constant diffusivity.
3) The vertical profile of soil textures, which determines the conductivity and potential functions, is defined for each 8° × 10° gridbox according to soil type, as prescribed by the 1° × 1° soil file and profile descriptions developed by Zobler (1986; 1985). Model II's soil characteristics were specified by vegetation type.
4) Surface runoff is physically modeled, instead of prescribed.
5) The process of underground runoff is included and is physically modeled.
6) Gravitational potential is included.
7) Transpiration is included in evaporation from land surfaces.
8) Evaporation of intercepted precipitation and dew on the canopy is modeled.
9) Evaporation from bare soil is calculated separately from vegetation-covered surfaces.

2. Soil water movement

The distribution of water in the soil will be calculated in order to model accurately the processes of transpir-

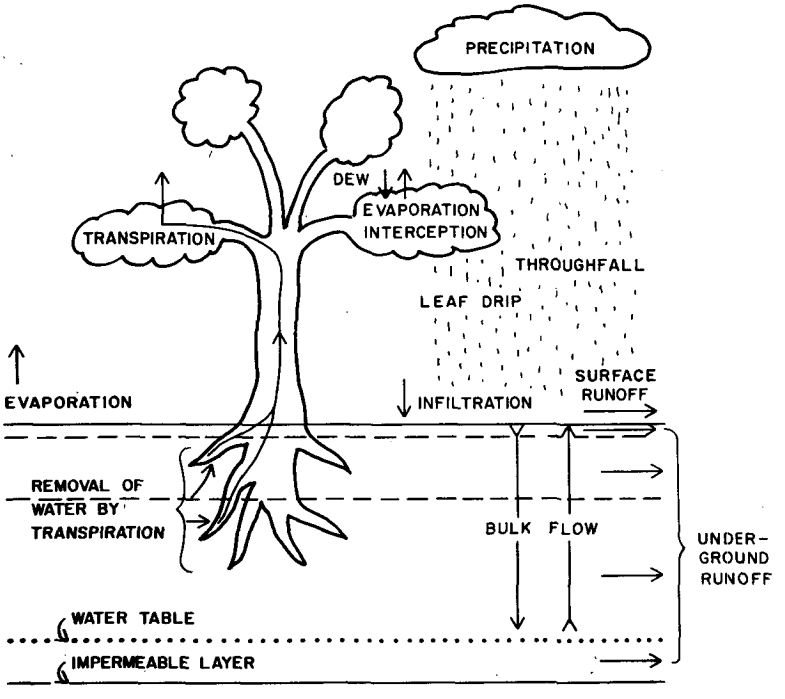

FIG. 1. Schematic of processes included in improved ground hydrology calculations.

ation, evaporation from soil, runoff, and heat transport within the soil. Each of these processes significantly affects the heat exchange between the atmosphere and the surface; consequently, an accurate modeling of soil hydrology is an important part of long-term atmospheric modeling.

a. *Finite difference equations*

Darcy's law is assumed to hold throughout the soil:

$$F = -K\nabla(h + z), \tag{1}$$

where F is the water flux, K the hydraulic conductivity, h the matric potential, and z the depth. The vertical component of this equation is

$$F = -K\left(\frac{dh}{dz} + 1\right). \tag{2}$$

If h is a function of the volumetric moisture content, θ, then (2) can be rewritten as

$$F = -\left(D\frac{d\theta}{dz} + K\right), \tag{3}$$

where D, the diffusivity, is given by $Kdh/d\theta$. In order to handle cases of soil profiles with horizons consisting of various textures, the matric potential must be considered a function of z as well as θ. In this case, dh/dz can no longer be written as $(dh/d\theta)(d\theta/dz)$ as in (3), but must be represented as

$$\frac{dh}{dz} = \frac{\partial h}{\partial \theta}\frac{d\theta}{dz} + \frac{\partial h}{\partial z}. \tag{4}$$

The flux equation now cannot be written in the diffusion form (3), due to the presence of $\partial h/\partial z$. We use (2) to describe the flux since soil profiles are generally heterogeneous. Each layer, however, is assumed to be of uniform texture.

Numerical methods were first used to solve the homogeneous case by Hanks and Bowers (1962). These methods were extended to the heterogeneous case by Wang and Lakshminarayana (1968). Our model uses the following finite difference form of Darcy's law (see Fig. 2):

$$F_l = K_l(H_l - H_{l-1})/(Z_l - Z_{l-1}), \tag{5}$$

where F_l is the flux between layers l and $l-1$, K_l is the hydraulic conductivity between layers l and $l-1$, H_l is the total potential (matric plus gravitational) of layer l, and Z_l is the mean depth of layer l. The surface is initially assumed to be level, with the layers parallel to the surface. We will let our dependent variable be w_l, the quantity of water in layer l. Flux in the upward direction is positive, so the equation for w_l is

$$\frac{dw_l}{dt} = F_{l+1} - F_l. \tag{6}$$

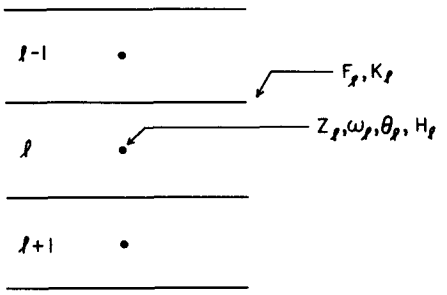

FIG. 2. The soil model layers. Quantities F_l and K_l are defined at the boundaries; the remaining quantities are defined at the centers. Index l refers to the layer and its upper boundary.

b. *Time scheme*

In order to ensure numerical stability of the solution, an implicit time scheme is used. The form of the scheme is

$$w_l^{n+1} = w_l^n + (F_{l+1}^{n+\alpha} - F_l^{n+\alpha})\Delta t, \tag{7}$$

where the superscripts indicate the time step, and α is a parameter between 0 and 1. This can be written more compactly, with a change in notation, as

$$\Delta w_l = (F_{l+1}^{\alpha} - F_l^{\alpha})\Delta t. \tag{8}$$

Here F_l^{α} is the flux evaluated at a time intermediate between the present time step and the next time step. Equation (8) can be solved approximately by linearizing with respect to Δw_l, or it can be solved exactly with a Newton–Raphson iteration. In either case, the solution is facilitated because the equations can be cast in tridiagonal form [see (5)], yielding a rapid solution via the Gauss–Jordan algorithm. Equation (8) does not include effects of hydraulic pressure under saturated conditions, underground runoff, or evapotranspiration, and must be modified to include these processes. These changes are discussed here.

c. *Boundary conditions*

If L is the number of layers, the boundary condition at the bottom is taken to be one of

$$\left.\begin{array}{ll} \text{a:} & F_{L+1} = 0 \\ \text{b:} & F_{L+1} = -K_{L+1} \end{array}\right\}. \tag{9}$$

Case (a) is for the presence of bedrock, while case (b) represents gravitational drainage of water when bedrock is below the bottom boundary. Depth to bedrock is prescribed for the soil units of the Zobler world soil file according to profile descriptions (FAO 1974).

The boundary condition at the top is taken to be the minimum of the precipitation and infiltration capacity, or infiltrability,

$$F_1 = -\min(P_r, I_{\max}), \tag{10}$$

where P_r is the precipitation rate and $I_{\max}$, the infiltra-

tion capacity. Given that the top layer is assumed to be homogeneous, I_{max} can be calculated as

$$I_{max} = K_1(w_{sat})\left[\left.\frac{dh_1}{dw_1}\right|_{w_1=w_{sat}} \frac{(w_1 - w_{sat})}{Z_1} + 1\right], \quad (11)$$

where w_{sat} is the saturation value of w_1, and h_1 is the matric potential in layer 1. Rainfall not entering the soil is removed as surface runoff. The GISS GCM rainfall intensities appear to be low; therefore a subgrid-scale parameterization of rainfall intensity and areal variability may be included in a later version of the model.

d. Underground runoff

If the surface is not level, but at an angle χ from the horizontal, then (2) splits into two components,

$$\left.\begin{aligned} &\text{a:} \quad F_z = -K\left[\frac{dh}{dz} + \cos(\chi)\right] \\ &\text{b:} \quad F_y = -K\sin(\chi) \end{aligned}\right\}, \quad (12)$$

where z now represents the perpendicular distance below the surface and y is a coordinate perpendicular to z in the uphill direction. The vertical flux equation is therefore essentially the same as before, but now a horizontal flux equation,

$$F_y = -KS, \quad (13)$$

where $S = \sin\chi$, has been added.

We next assume that there are sinks which can remove water that is moving horizontally. If these sinks occur at a distance δ apart, we can calculate the overall loss of water to the sinks as follows: Considering the region between two sinks and ignoring any vertical transport of water, the flux entering the region from the uphill side is zero, while the flux leaving the region on the downhill side is F_y. For layer l, the mass of water leaving a square area of side δ per unit time is $F_y\delta\Delta Z_l$, where ΔZ_l is the thickness of layer l. Consequently,

$$\frac{dw_l}{dt} = F_y\frac{\Delta Z_l}{\delta} \quad (14)$$

is the change in water content in layer l due to underground runoff.

The surface slope, χ, is prescribed for each 1° cell from the Zobler world soil file and composited for the 8° × 10° gridbox by weighted average. The distance between sinks, δ, is related to the mean interstream distance and is prescribed for each gridbox.

e. Complete soil equations

Equation (6) can now be modified to take into account both underground runoff and evapotranspiration. Thus,

$$\frac{dw_l}{dt} = F_{l+1} - F_l - \frac{\bar{K}_l S\Delta Z_l}{\delta} - \mathrm{ET}_l, \quad (15)$$

where F_l is the z component of the flux at boundary l, $\bar{K}_l$ the mean conductivity in layer l, and ET_l the evapotranspiration from layer l.

f. Soil water functions, classifications, and characteristics

The hydraulic conductivity $K(\theta)$ and the matric potential $h(\theta)$ (Fig. 3) were obtained by fitting the following functional form to observed data:

$$\exp(a_{-1}\theta^{-1} + a_0 + a_1\theta + a_2\theta^2). \quad (16)$$

The fits were done by the method of least squares in the logarithm of h or K. The coefficients are functions of the soil texture. The matric potential curves and

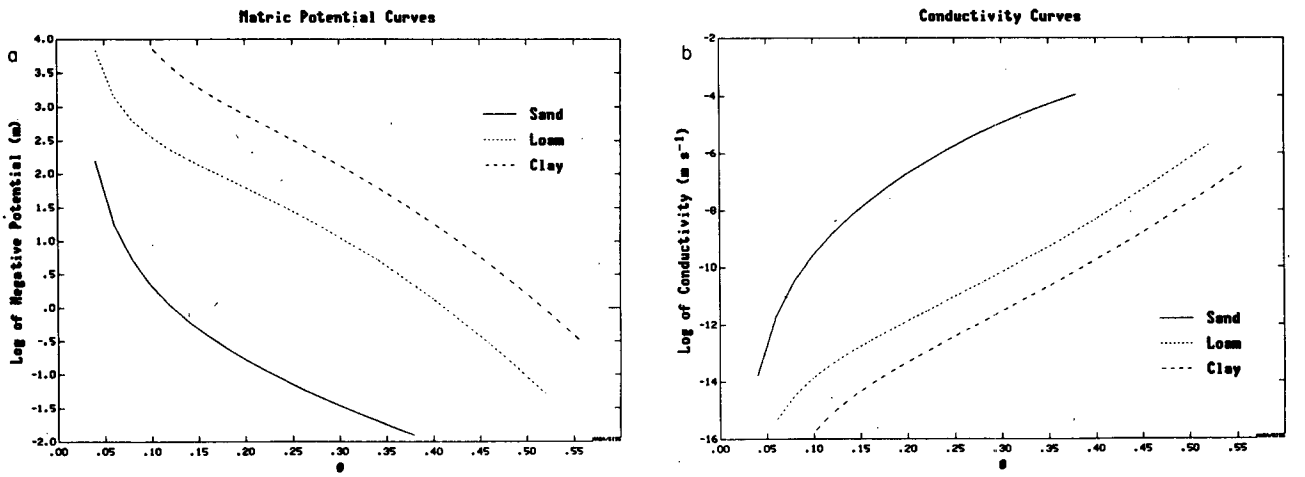

FIG. 3. Theta-matric potential (a) and theta-conductivity (b) curves for sand, loam, and clay texture classes.

saturated conductivities for the three (coarse, medium, and fine) textures were supplied by Zobler (personal communication 1985). The conductivity curves were then determined by the method of Mualem (1976). The effects of soil structure on the hydraulic properties may be included in a later version of the model.

The soil water functions are considered to be functions of the water content. However, although both the matric potential and the hydraulic conductivity display a hysteresis effect (Hillel 1982), this is neglected in the interest of simplicity.

g. *Compositing*

A layer may contain more than one distinct horizon, so that different soil textures, with distinct matric potentials and conductivities, are present. The soil data consist of horizons, defined in terms of their depths and textures, on a 1° × 1° grid, according to FAO (1974) descriptions. In general, the horizon boundaries will not be aligned with the model layers, so that an averaging of the soil properties in the vertical must be done. Each 1° × 1° cell is therefore divided vertically into model layers, consisting of one or more horizons. The model grid size will usually be either 8° × 10° or 4° × 5°, so that an averaging of the soil properties in the horizontal is necessary as well.

A θ_{sat} is calculated for each 1° × 1° layer by taking the weighted average of the θ_{sat} for each texture within the layer. A relative moisture content, equal to θ/θ_{sat}, is then used to evaluate the hydraulic conductivities and matric potentials for each of the textures. The composite matric potential in the 8° × 10° layer is evaluated by taking the weighted average of the potentials within the 1° × 1° layer, and the weighted average of these averages over the 8° × 10° gridbox. The composite matric potential is expressed as a linear sum of the potentials of each of the textures.

The conductivities of each 1° × 1° layer should be calculated on the basis of the weighted harmonic mean, in analogy with series electrical resistors. Then the composite 8° × 10° layer conductivity can be calculated by taking the weighted average of the 1° × 1° layer conductivities, in analogy with parallel electrical resistors.

However, in order to carry out the foregoing averaging procedure for the conductivities, the model would require calculations on the 1° × 1° grid at each time step. In order to avoid this, the harmonic mean of the conductivity for each 1° × 1° layer is approximated by retaining only the term that would dominate at saturation. In this approximation, the conductivity of each 1° × 1° layer is proportional to the conductivity of a single texture. As a result, the composite conductivity of each 8° × 10° layer can be written as a linear sum of the conductivities of each texture.

The conductivities that are directly calculated represent the mean conductivities within the given layers. In order to carry out the water movement calculations, the conductivities at the interface between layers are needed. We obtained the between-layer conductivities by interpolating the two neighboring mean conductivities to the interface.

Two methods of interpolating the conductivities were tried. The first used linear interpolation and the second used geometric, or logarithmic, interpolation. These two methods were tested by observing the infiltration for a rainfall rate of 5×10^{-6} m s^{-1} over clay (Fig. 4). The infiltration rate for three soil layers is compared to results for six- and twelve-layer models. These results show that both methods of interpolation result in an overestimate of the infiltration for the three-layer case. The geometric interpolation is somewhat

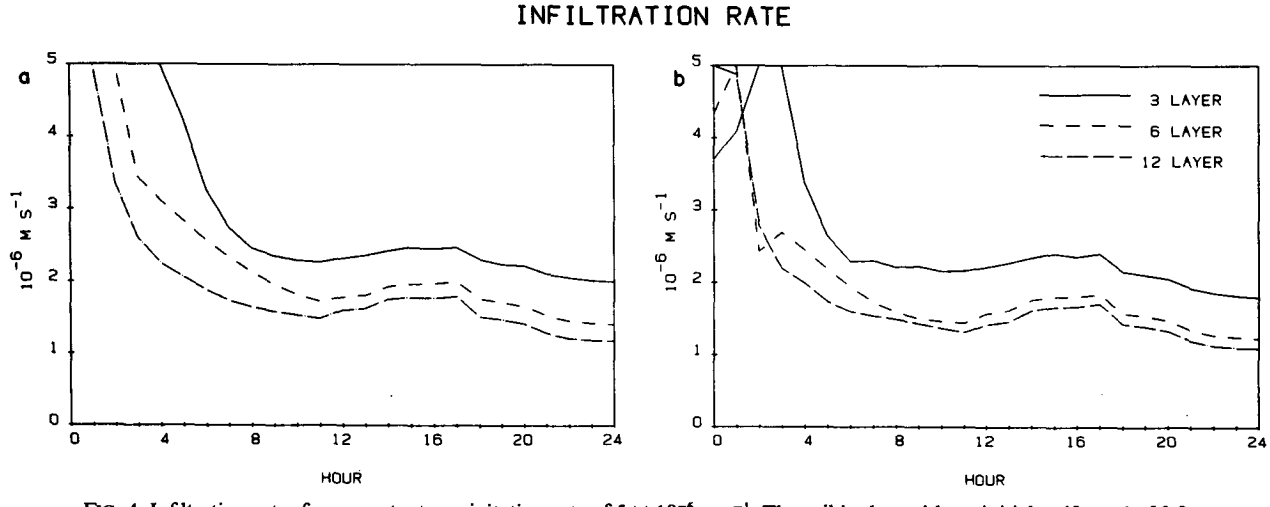

FIG. 4. Infiltration rates for a constant precipitation rate of 5×10^{-6} m s^{-1}. The soil is clay, with an initial uniform θ of 0.3. Linear interpolation results are shown in (a); geometric interpolation is shown in (b).

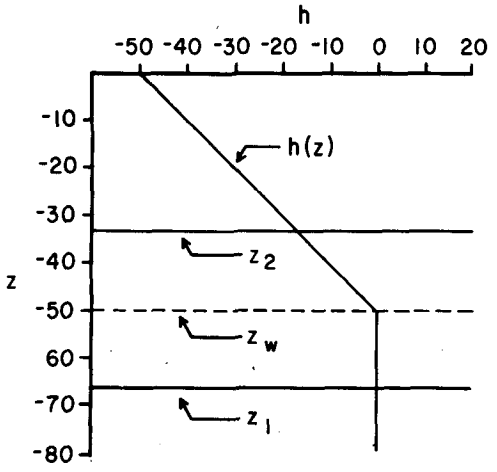

FIG. 5. The matric potential in the vicinity of the water table, z_w.

more accurate in terms of the accumulated infiltration, but can suffer from oscillations. At present, the geometric interpolation method is used to evaluate the conductivity, but other methods are being examined, such as interpolating θ rather than the conductivity.

h. Layering

Three soil layers are used in the model. The thicknesses of the layers are in a geometric series. For this version of the model, the top layer is taken to be 0.08 m thick, and the bottom boundary is located either at 3.44 m or at the depth of the bedrock, if bedrock is present at a shallower depth. If bedrock is not present to a depth of 3.44 m, the bottom boundary is considered to be permeable.

Although three soil layers are used in this version, the model can be run with any number of soil layers (see Fig. 4). When linked to a GCM, the number of layers will be chosen in such a way as to yield a reasonable compromise between accuracy and computational cost.

i. Position of the water table

The water table, defined as the position of the boundary between saturated and unsaturated soil, is an important quantity in describing and understanding soil water processes, but it is not a prognostic variable of the soil model. Instead, it is calculated separately based on the quantities of water in each of the three soil layers (see appendix A). The location of the water table can be estimated to an accuracy significantly greater than the spacing between soil layers.

The water table is found in the lowest unsaturated soil layer. The water table's depth within a given layer can be approximated by

$$z_w = z_2 - [-2\bar{h}(z_1, z_2)(z_2 - z_1)/(q(z_w, z_2) + 1)]^{1/2}, \quad (17)$$

where z_1 and z_2 are the lower and upper layer boundaries, respectively, $\bar{h}(z_1, z_2)$ is the average matric potential in the layer (Fig. 5), and

$$q(z_w, z_2) \approx F(z_2)/K[\theta(z_2)]. \quad (18)$$

3. Evapotranspiration

For the evapotranspiration calculations, we consider the vegetation to exist in a pseudosurface layer, with negligible heat capacity. Precipitation and dew are partitioned into throughfall and interception through the use of a landcover fraction and a canopy storage capacity. Evapotranspiration is then divided areally into three parameters (Fig. 6): 1) transpiration from dry vegetation; 2) evaporation of intercepted precipitation or dew on the canopy; and 3) evaporation from bare soil. The soil surface shaded by vegetation does not evaporate.

a. Transpiration from vegetation with dry canopy

The equation for unstressed transpiration, T_{unst}, is based on Monteith (1981):

$$T_{\text{unst}} = f_d[\Delta R_n + c_p \rho J(e_a - e_d)/R_a]/ [\Delta + \gamma(1 + R_c/R_a)]\lambda, \quad (19)$$

where f_d is the fraction of canopy which is dry, Δ the slope of the saturated vapor pressure curve at the surface plane temperature T_s, R_n the net radiation, c_p the specific heat of air at constant pressure, ρ the density of air, J the mechanical equivalent of heat, e_a the saturation vapor pressure at T_s, e_d the vapor pressure at the surface plane, R_a the atmospheric boundary layer resistance to vapor transfer from the canopy to the surface plane, R_c the canopy resistance, γ the psychrometric constant, and λ the latent heat of vaporization.

Equation (19) gives essentially the same answer as the aerodynamic formula. It has the advantage that it is easily adapted to off-line models. When linked to a GCM, (19) or the corresponding aerodynamic formula

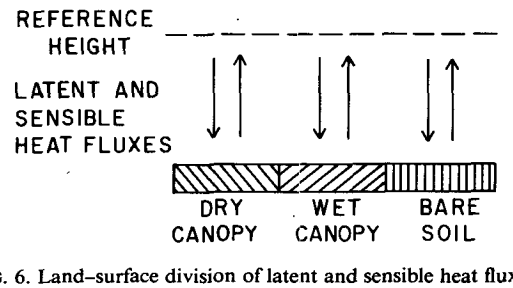

FIG. 6. Land–surface division of latent and sensible heat fluxes.

will be involved in an iterative time-step procedure (see section 2e).

All of the foregoing quantities except for R_c and f_d can be obtained directly from the GCM atmospheric variables. The boundary layer resistances to vapor transfer for cases of neutral and nonneutral stability are calculated as in the present model II, with the difference that a zero plane displacement value is specified in addition to surface roughness. The zero plane displacement, which is important in calculating boundary layer resistance for very tall vegetation types, is calculated according to Monteith (1973):

$$\mathrm{ZD} = 0.63\ \mathrm{VH}, \tag{20}$$

where VH is the vegetation height. Surface roughness of vegetation is calculated according to Monteith (1973):

$$\mathrm{ZO} = 0.13\ \mathrm{VH}. \tag{21}$$

These are used in the calculation of the drag coefficient, C_D. The boundary layer resistance is related to the drag coefficient by

$$R_a = 1/(V_s C_h), \tag{22}$$

where V_s is the wind speed at the surface plane, and C_h the humidity transfer coefficient, which is related to C_D and the Richardson number (Hansen et al. 1983).

When the evapotranspiration calculations are incorporated into the GCM, the surface roughness will be determined as in model II as the maximum of topographic or vegetation surface roughness, since effective surface roughness depends on both large-scale topography and small-scale surface texture.

The canopy resistance describes the vegetative control of water loss to the atmosphere. In the model, it is calculated as a bulk stomatal resistance estimated for the evaporating leaf surfaces treated as parallel resistors (Fig. 7):

$$R_c = \frac{r_s}{\mathrm{LAI}_e}, \tag{23}$$

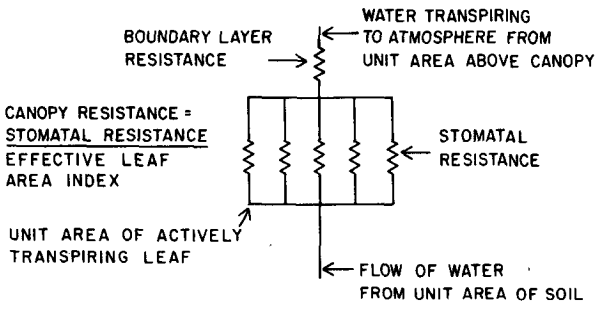

FIG. 7. Canopy resistance portrayed as a parallel resistor system, in series with the boundary layer resistance. Each conductor represents one unit area of actively transpiring leaf. The sum of the actively transpiring leaf unit areas equals the effective leaf area index.

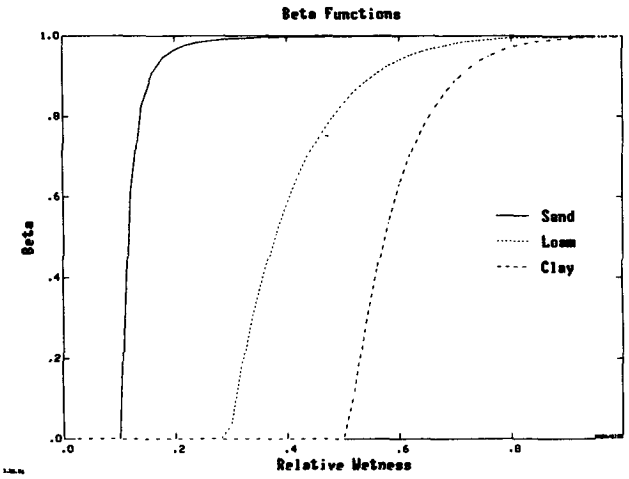

FIG. 8. Soil water availability (β_w) functions for sand, loam, and clay.

where r_s is minimum stomatal resistance and LAI_e is the effective leaf area index, defined as the projected area of evaporating leaves per unit area of ground. The use of minimum stomatal resistance overestimates transpiration rate since stomatal resistance varies with light, temperature, and humidity; functional relationships for these effects may be incorporated in the model later. The LAI_e is calculated as a function of LAI:

$$\mathrm{LAI}_e = \mathrm{LAI}_c[1 - \exp(-\mathrm{LAI}/\mathrm{LAI}_c)], \tag{24}$$

where LAI_c is the maximum value of LAI_e. Effective LAI is used to account for the attenuation of radiation as light passes through the canopy and the coincident decrease in plant surface which is actively transpiring (Aston 1984).

The actual transpiration from each soil layer T_l, is calculated as the product of total unstressed transpiration, T_{unst}, soil moisture availability in layer l, $\beta_w(l)$, and fraction of roots present in soil layer l, $f_r(l)$:

$$T_l = f_r(l)\beta_w(l)T_{\mathrm{unst}}. \tag{25}$$

Total transpiration, T, is the sum of T_l over all layers. Actual flow of water from the soil to the leaves depends on soil water potential, resistance of water flow to the root surface, specific resistance of system elements, and leaf water potential. The soil moisture availability factor, β_w, is used to approximate this flow and is taken to be linearly dependent on the total potential in each soil layer (Fig. 8),

$$\beta_w(l) = \max\left(\frac{H_w - H_l}{H_w}, 0\right), \tag{26}$$

where H_w is the wilting point. Although (25) looks like a simple bucket model, the use of (26) yields more realistic transpiration rates, due to the nonlinear dependence of transpiration on θ.

Cumulative root distribution functions were developed for different vegetation types based on observations of root distribution, length (used as a proxy for root surface area), and depth reported in the literature. Sources of root data include Odum and Pigeon (1970), Epstein (1973), Kutschera (1960), Klinge (1973), and Collinson (1977). The functions were fit using the form,

$$F(z) = az^b, \tag{27}$$

where z is the depth of soil layer and a and b are coefficients. The fraction of roots present in each soil layer, $f_r(l)$, is determined from the difference in the cumulative root distribution functions at the top and bottom of each layer.

b. Evaporation of intercepted precipitation and dew

Interception of rainfall by vegetation can amount to a significant fraction of precipitation, as much as 15–40 percent in coniferous forests (Rutter 1975). The intercepted water eventually evaporates from the leaves, and is not available for runoff or transpiration; it also suppresses transpiration from the wet surface of the canopy. Therefore, as Dickinson (1984) has argued, interception should be included in ground hydrology models for GCMs.

Canopy water storage capacity, w_{sc}, in kg m^{-2}, is defined as

$$w_{sc} = 0.1 \text{ LAI}. \tag{28}$$

Precipitation intercepted by the canopy is subtracted from precipitation. If the sum of dew and intercepted precipitation, w_c, is greater than w_{sc}, the excess is added to precipitation. The fraction of canopy which is wet, f_w, is calculated as in Deardorff (1978):

$$f_w = (w_c/w_{sc})^{2/3}. \tag{29}$$

The fractional power in (29) allows for simulation of water covering the entire canopy during formation of dew and only part of the canopy during evaporation. It also allows for complete drying of the canopy. Evaporation of w_c is calculated using the Penman (1948) equation, since no vegetational resistance is present:

$$E_{wc} = \begin{cases} f_w[\Delta R_n + c_p\rho J(e_a - e_d)/R_a]/(\Delta + \gamma)\lambda, & E_{wc} > 0 \\ [\Delta R_n + c_p\rho J(e_a - e_d)/R_a]/(\Delta + \gamma)\lambda, & E_{wc} < 0. \end{cases} \tag{30}$$

Dew occurs when E_{wc} is negative.

c. Evaporation from bare soil

Evaporation from bare soil, E, is taken to be the minimum of the Penman (1948) formulation for potential evaporation, E_p, and the formula for maximum evaporation, $E_{\max}$, of Gardner and Hillel (1962):

$$E = \min(E_p, E_{\max}). \tag{31}$$

Assuming that relative humidity at the soil surface equals 1, the Penman (1948) formula for E_p is

$$E_p = [\Delta H_0 + c_p\rho J(e_a - e_d)/R_a]/(\Delta + \gamma)\lambda, \tag{32}$$

where H_0 is the net heat at surface. The Gardner and Hillel (1962) formula for $E_{\max}$ is

$$E_{\max} = \frac{D_1\theta_1\pi^2}{4\Delta Z_1}, \tag{33}$$

where D_1 is the diffusivity of the first soil layer.

d. Evapotranspiration

Potential evapotranspiration, ET_p, is calculated as

$$\text{ET}_p = f_v T_{\text{unst}} + (1 - f_v)E_p + f_v E_{wc}. \tag{34}$$

Actual evapotranspiration, ET, is calculated as

$$\text{ET} = f_v T + (1 - f_v)E + f_v E_{wc}. \tag{35}$$

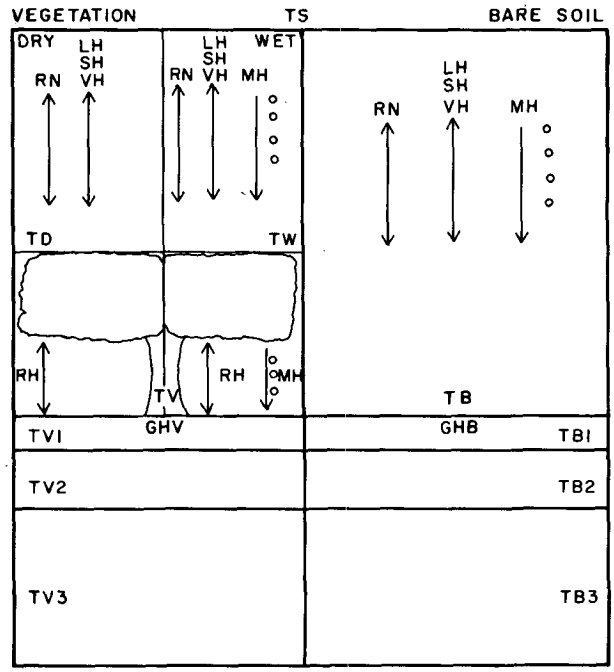

FIG. 9. Proposed energy balance and temperature components of the ground hydrology model for coupling to the GCM. RN: net radiation, LH: latent heat flux, SH: sensible heat flux, VH: heat of water vapor, MH: heat of water, TD: temperature of dry canopy, TW: temperature of wet canopy, RH: radiative heat between ground and canopy; TV: temperature of vegetated portion of land surface below canopy, TB: temperature of bare soil, GHV: ground heat flux of vegetated portion of land surface, GHB: ground heat flux of bare soil, TV1, TV2 and TV3: temperatures of three model soil layers of vegetated portion of land surface, TB1, TB2 and TB3: temperatures of three model soil layers beneath bare soil portion of land surface.

e. Energy balance and links to the GISS GCM

In the GISS GCM the latent and sensible heat fluxes from the surface layer to the first layer depend on both temperature and water vapor mixing ratio. The GCM assumes that the flux into the surface layer from the ground equals the flux from the surface layer into the first layer, for both latent and sensible heats. This yields a set of simultaneous equations which are solved for surface temperature and water-vapor mixing ratio. A similar procedure will be followed in coupling the hydrology model to the GCM.

The hydrology model divides the net heating of the evaporating land surface into latent and sensible heat fluxes. The Penman–Monteith equations calculate the portion of net heating which occurs as the latent heat flux. The sensible heat flux is equal to the difference between the net heating and the latent heat flux. The partitioning of latent and sensible heat fluxes implies the temperature of the evaporating surface, and this temperature in turn affects the net heating of that surface and the boundary layer resistance. Consequently, the temperature of the evaporating surface must simultaneously satisfy the latent heat, radiation, ground heat, and aerodynamic relationships. Proposed energy balance and temperature components of the ground hydrology model for coupling to the GCM are shown in Fig. 9.

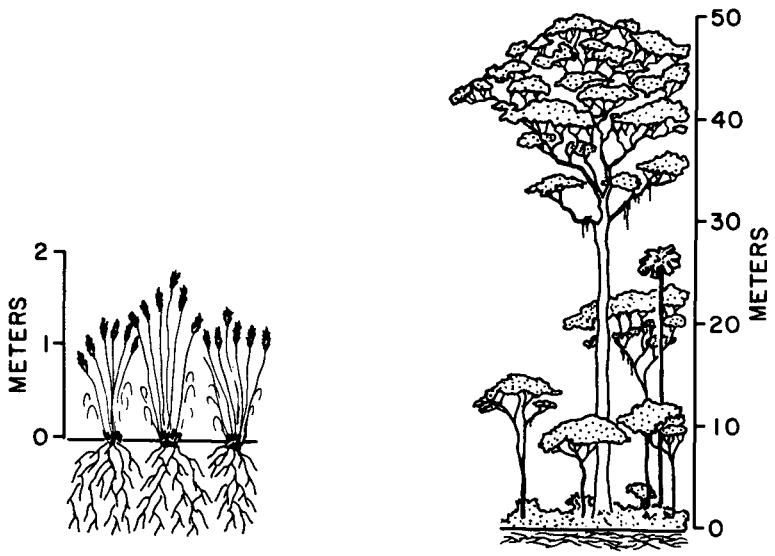

	GRASSLAND		TROPICAL RAINFOREST	
Max. LAI	2.9	Prentice, 1985	12.0	Prentice, 1985
Mean Max. Height (m)	2.0	UNESCO, 1973	51.0	Schulze, 1982
Min. Stomatal Resistance ($s\ m^{-1}$)	94.0	Korner et al., 1979	287.5	Fetcher et al., 1983
Canopy Resistance* ($s\ m^{-1}$)	42.7		45.1	
Land Cover Fraction	0.82	Geiger, 1965	0.95	Shuttleworth et al., 1984
Max. Interception Storage Capacity** ($kg\ m^{-2}$)	0.29		1.2	

*Canopy Resistance = $\frac{\text{Stomatal Resistance}}{LAI_e}$, $LAI_c = 5.0$.

**Interception Storage Capacity = 0.1 x LAI .

FIG. 10. Vegetation characteristics for two contrasting vegetation types.

TABLE 1. Soil and vegetation combinations for four gridboxes.

Number	Soil type–vegetation type	
	A. Sahel	
1	ferric luvisol	trop.-subtrop. evergreen seasonal broadleaf forest
1	eutric regosol	trop.-subtrop. evergreen seasonal broadleaf forest
2	ferric acrisol	tall-med.-short grassland, 10–40% woody tree cover
1	lithosol	tall-med.-short grassland, 10–40% woody tree cover
2	eutric fluvisol	tall-med.-short grassland, 10–40% woody tree cover
4	ferric luvisol	tall-med.-short grassland, 10–40% woody tree cover
1	gleyic luvisol	tall-med.-short grassland, 10–40% woody tree cover
1	eutric nitosol	tall-med.-short grassland, 10–40% woody tree cover
5	cambic arenosol	tall-med.-short grassland, 10–40% woody tree cover
5	luvic arenosol	tall-med.-short grassland, 10–40% woody tree cover
2	eutric regosol	tall-med.-short grassland, 10–40% woody tree cover
1	chromic vertisol	tall-med.-short grassland, 10–40% woody tree cover
1	pellic vertisol	tall-med.-short grassland, 10–40% woody tree cover
1	solodic planosol	tall-med.-short grassland, 10–40% woody tree cover
1	orthic acrisol	tall-med.-short grassland, 10% woody tree cover
3	lithosol	tall-med.-short grassland, 10% woody tree cover
1	eutric fluvisol	tall-med.-short grassland, 10% woody tree cover
11	ferric luvisol	tall-med.-short grassland, 10% woody tree cover
1	gleyic luvisol	tall-med.-short grassland, 10% woody tree cover
3	plinthic luvisol	tall-med.-short grassland, 10% woody tree cover
4	dystric nitosol	tall-med.-short grassland, 10% woody tree cover
2	luvic arenosol	tall-med.-short grassland, 10% woody tree cover
2	eutric regosol	tall-med.-short grassland, 10% woody tree cover
2	pellic vertisol	tall-med.-short grassland, 10% woody tree cover
1	orthic solonchak	tall-med.-short grassland, 10% woody tree cover
1	rhodic ferralsol	tall-med.-short grassland, shrub cover
2	ferric luvisol	tall-med.-short grassland, shrub cover
2	dystric nitosol	tall-med.-short grassland, shrub cover
5	cambic arenosol	tall-med.-short grassland, shrub cover
6	luvic arenosol	tall-med.-short grassland, shrub cover
1	pellic vertisol	tall-med.-short grassland, shrub cover
1	lithosol	tall grassland, no woody cover
1	eutric fluvisol	medium grassland, no woody cover
	B. India	
2	chromic luvisol	trop.-subtrop. evergreen seasonal broadleaf forest
1	chromic vertisol	trop.-subtrop. evergreen seasonal broadleaf forest
1	vertic cambisol	trop.-subtrop. drought-deciduous forest
3	lithosol	trop.-subtrop. drought-deciduous forest
1	calcaric fluvisol	trop.-subtrop. drought-deciduous forest
9	chromic luvisol	trop.-subtrop. drought-deciduous forest
10	ferric luvisol	trop.-subtrop. drought-deciduous forest
8	eutric nitosol	trop.-subtrop. drought-deciduous forest
18	chromic vertisol	trop.-subtrop. drought-deciduous forest
6	pellic vertisol	trop.-subtrop. drought-deciduous forest
1	chromic luvisol	xeromorphic forest-woodland
4	chromic vertisol	xeromorphic forest-woodland
3	pellic vertisol	xeromorphic forest-woodland
1	ferric luvisol	trop.-subtrop. drought-deciduous woodland
1	chromic vertisol	trop.-subtrop. drought-deciduous woodland
	C. Brazil	
1	plinthic acrisol	tropical evergreen rainforest
11	orthic ferralsol	tropical evergreen rainforest
48	xanthic ferralsol	tropical evergreen rainforest
16	dystric gleysol	tropical evergreen rainforest
1	lithosol	tropical evergreen rainforest
3	ferralic arenosol	tropical evergreen rainforest
	D. Sahara	
22	lithosol	desert
2	calcaric fluvisol	desert
2	calcaric regosol	desert
1	eutric regosol	desert
52	haplic yermosol	desert
1	gypsic yermosol	desert

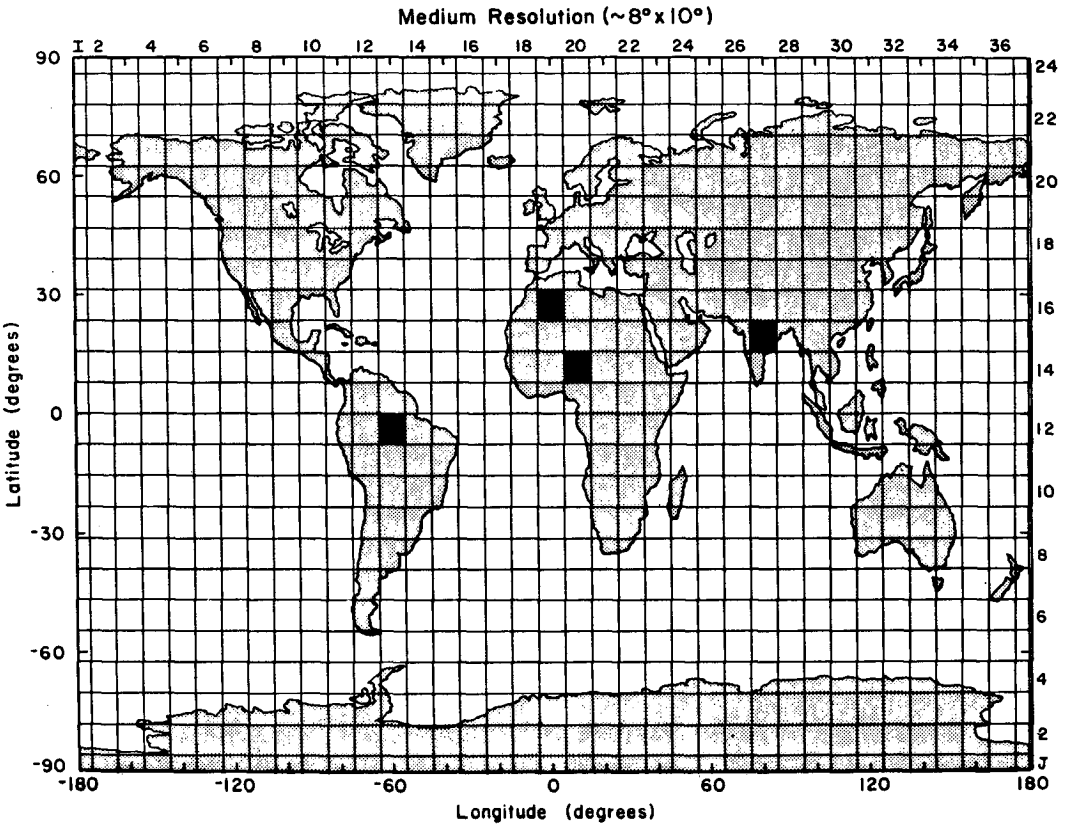

FIG. 11. Locations of test gridboxes.

f. Vegetation classification, characteristics, and compositing

For the evapotranspiration calculations, 32 classifications of the 178 vegetation types of the Matthews' global 1° × 1° vegetation dataset are used (Matthews 1983, 1984). The evapotranspiration calculations require information on leaf area index (LAI), stomatal resistance, vegetation height, root density and depth, landcover fraction and interception storage. Values for these characteristics as a function of vegetation type are specified from the literature, some of the more useful sources being Schulze (1982) for vegetation height and Körner et al. (1979) for minimum stomatal resistance. Some examples of vegetation characteristics are shown in Fig. 10 for two contrasting types. Seasonality of vegetative growth is prescribed through monthly variation of LAI; LAI as a function of month was obtained by regressing published field measurements against climate data according to Prentice (personal communication 1985). Characteristics are specified for 32 vegetation types for off-line testing of the calculations and for 10–15 major ecosystems for inclusion into the larger global climate model. The composite vegetation inputs for LAI, vegetation height, fraction of roots in each soil layer and landcover fraction are calculated as weighted averages of the characteristics of each vegetation type from the 1° × 1° data occurring

TABLE 2. Annual evapotranspiration calculations done with weighted averages of 1° × 1° gridcells compared to those done with composite vegetation and soil characteristics.

Gridbox	Variable	Weighted average (g cm^{-2})	Composite (g cm^{-2})
Brazil	transpiration	81.5	81.2
	evaporation from bare soil	13.7	13.8
	evaporation from canopy	66.8	66.8
	evapotranspiration	162.1	161.8
Sahel	transpiration	53.8	13.2
	evaporation from bare soil	62.7	106.5
	evaporation from canopy	2.7	2.7
	evapotranspiration	119.2	122.4
Sahara	transpiration	0.0	0.0
	evaporation from bare soil	16.0	18.0
	evaporation from canopy	0.0	0.0
	evapotranspiration	16.0	18.0
India	transpiration	52.1	52.1
	evaporation from bare soil	66.7	67.4
	evaporation from canopy	16.8	16.8
	evapotranspiration	135.6	136.3

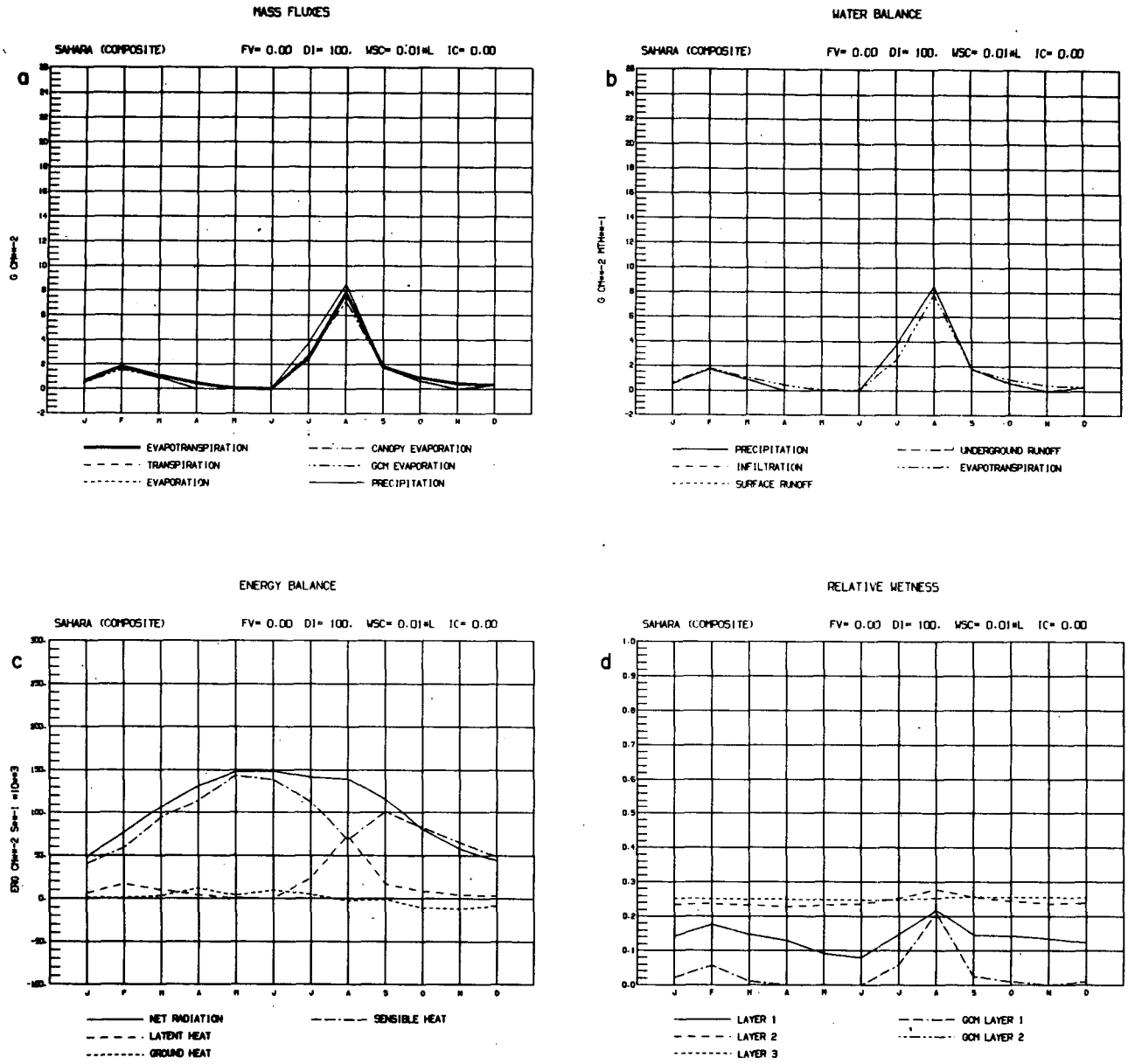

FIG. 12. Annual cycle of modeled evapotranspiration in the Sahara: (a) mass fluxes and GGM evaporation; (b) water balance; (c) energy balance; (d) relative wetness from ground hydrology model and GISS GCM Model II.

in the 8° × 10° gridbox. Composite boundary layer and canopy resistances are calculated as conductances and then inverted.

4. Results

a. Composite characteristics

An areally weighted average of evapotranspiration from each vegetation type and soil type combination at the 1° × 1° resolution was calculated over the 8° × 10° gridbox using GISS GCM Model II hourly data as inputs and then compared to evapotranspiration calculated by composite vegetation and soil characteristics. Locations of test gridboxes are shown in Fig. 11. Soil type and vegetation type combinations are shown in Table 1. Table 2 shows results from the four gridboxes. Comparisons show that evapotranspirations for 8° × 10° gridboxes calculated with composite vegetation and soil inputs are very close to the evapotranspirations calculated as weighted averages of the 1° × 1° cells except in the Sahel. In the Sahel, lower soil

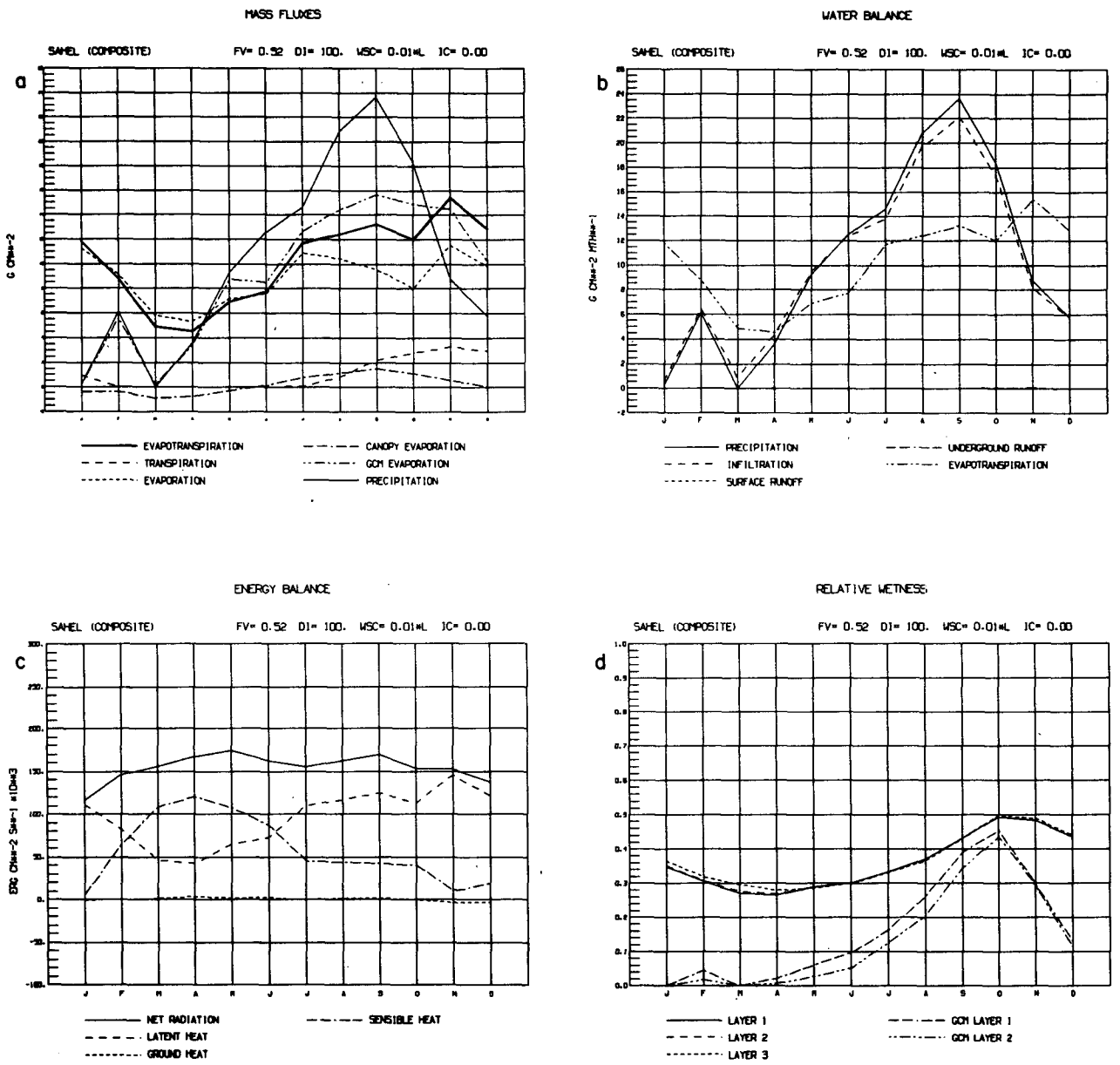

FIG. 13. Annual cycle of modeled evapotranspiration in the Sahel: (a) mass fluxes and GGM evaporation, (b) water balance, (c) energy balance, (d) relative wetness from ground hydrology model and GISS GCM Model II.

water levels produce more variability in the partitioning of evaporation between transpiration and evaporation from bare soil due to nonlinearity in the soil moisture availability factor curve (see Fig. 8). The Sahel gridbox has a heterogeneous land surface with numerous soil type and vegetation type combinations (see Table 1) which in concert with the lower soil water levels cause a discrepancy between weighted average and composite calculations. A smaller grid size would decrease this discrepancy, since the Sahelian region has latitudinal stratification of soil and vegetation types. The generally close results between weighted average and composite calculations justify the use of composite vegetation characteristics in the evapotranspiration calculations.

b. Test gridboxes

Diurnal and annual cycles of evapotranspiration were calculated using the improved ground hydrology model with GISS GCM Model II hourly data as inputs.

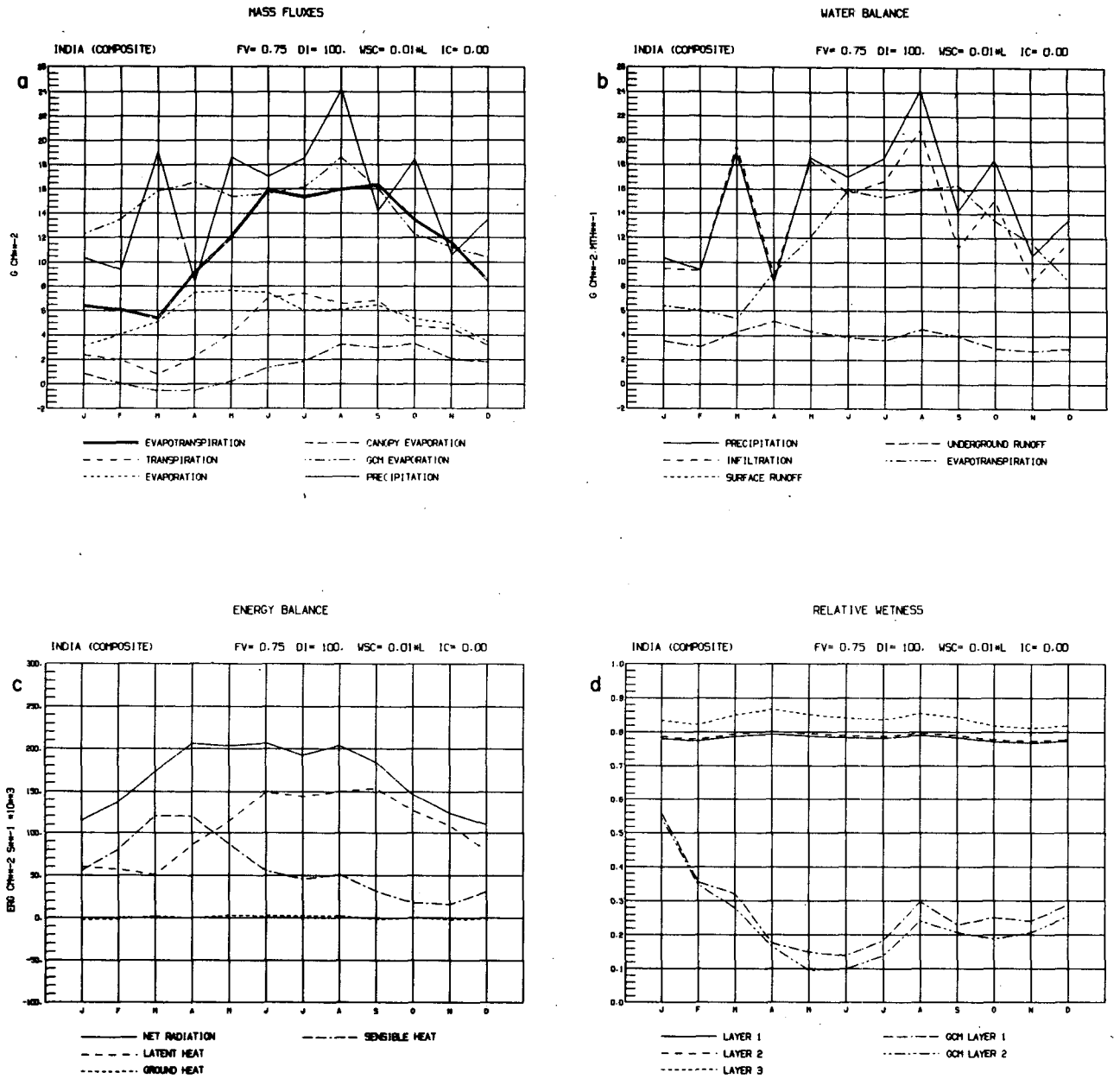

FIG. 14. Annual cycle of modeled evapotranspiration in India: (a) mass fluxes and GGM evaporation, (b) water balance, (c) energy balance, (d) relative wetness from ground hydrology model and GISS GCM Model II.

Annual cycles of evapotranspiration components, energy balance, water balance, and relative soil wetness calculated with composite vegetation and soil characteristics for the Sahara, Sahel and India gridboxes appear in Figs. 12–14 along with GISS GCM Model II precipitation, evaporation, and relative soil wetness. These figures show that the hydrology model responds appropriately to varying levels of precipitation in the different regions. The hydrology model has higher relative soil wetness than the GCM, due to the addition of canopy resistance to evaporation and to physically modeled soil moisture. Computed surface runoff values are low in the hydrology model, because local intensity of rainfall in the GCM is consistently low due to area averaging. The surface runoff curve in each case is masked by the zero grid line.

Results for the Brazilian rain forest gridbox are shown in Figs. 15 (diurnal cycle) and 16 (annual cycle);

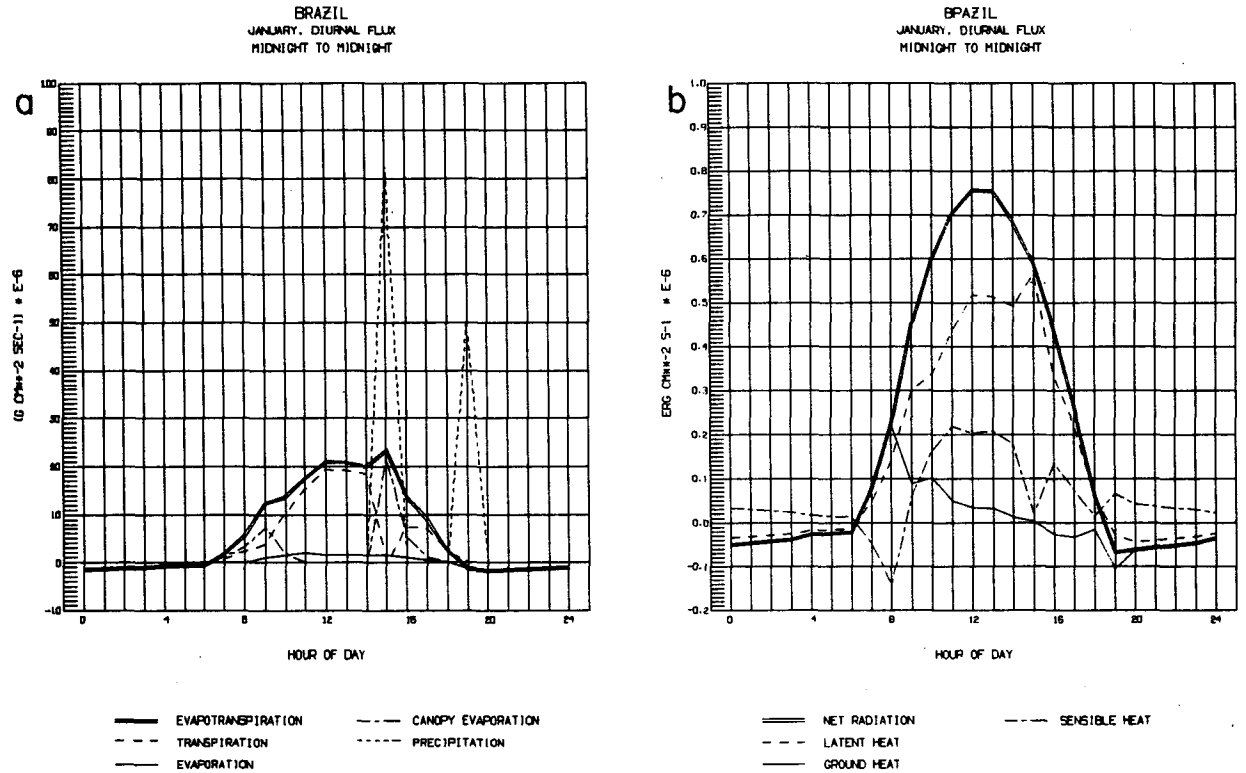

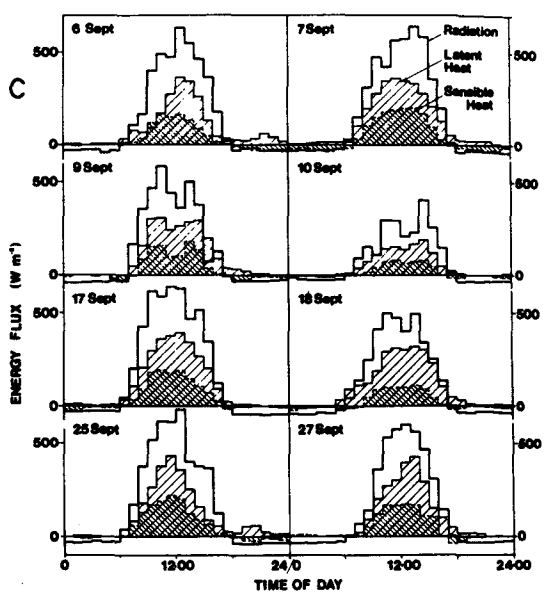

FIG. 15. Diurnal cycle of evapotranspiration for the Brazilian rainforest: (a) modeled mass fluxes, (b) modeled energy balance, (c) observed fluxes (Shuttleworth et al. 1984).

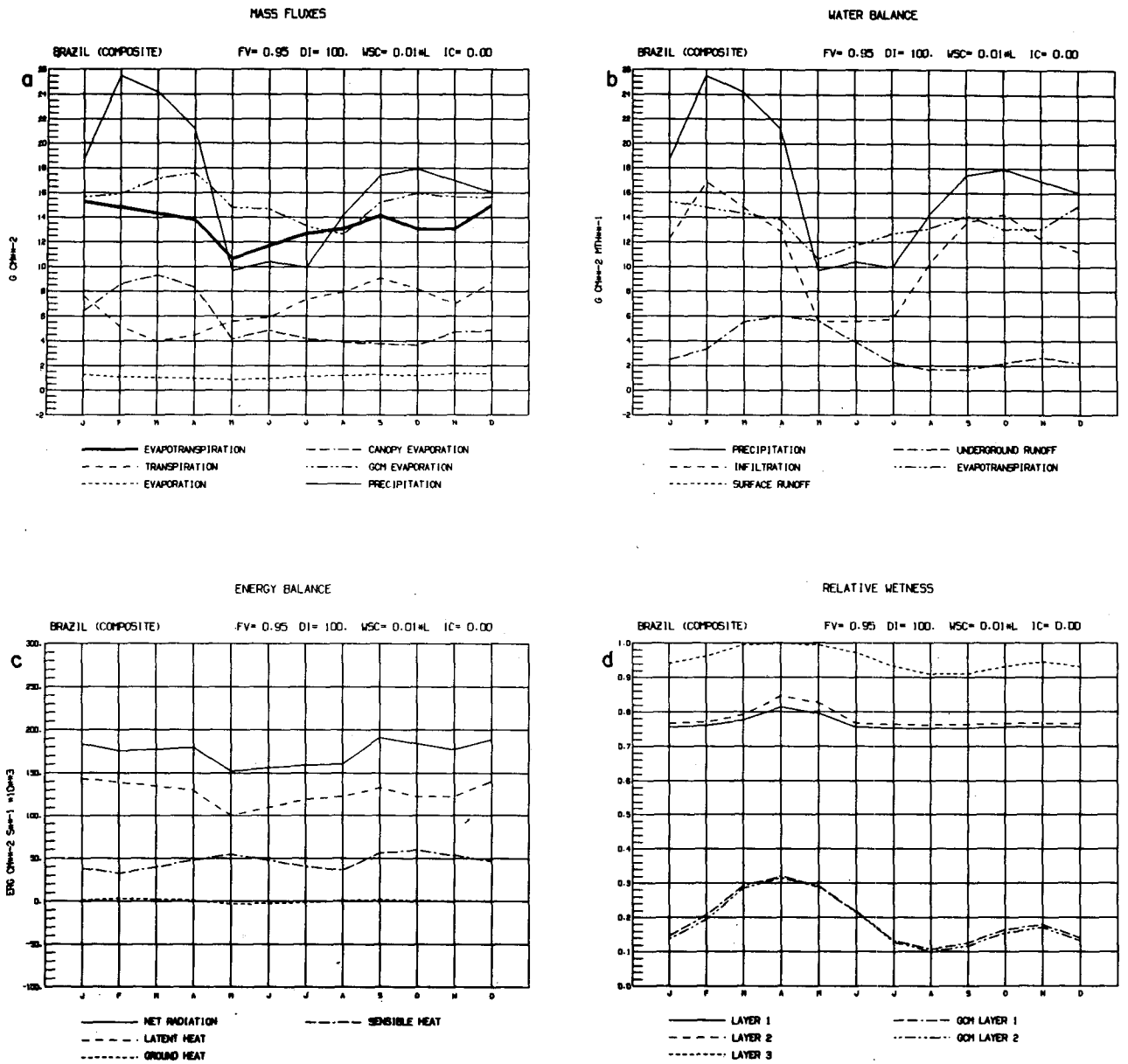

FIG. 16. Annual cycle of modeled evapotranspiration in the Brazilian rainforest: (a) mass fluxes and GGM evaporation, (b) water balance, (c) energy balance, (d) relative wetness from ground hydrology model and GISS GCM Model II.

observed values of the daily energy fluxes and annual water balance are shown for comparison. Modeled levels of diurnal net radiation, latent heat and sensible heat are approximately the same as observed fluxes. In addition, latent heat flux increases and sensible heat flux decreases in the morning when dew is evaporating and during rainfall events in a realistic manner. Modeled water balance is compared to observed water balance from a study of a model basin near Manaus, Brazil (Salati and Vose 1984) in Fig. 17. In general, modeled annual hydrological variables compare well with observed values; evaporation from bare soil, canopy evaporation, and total evapotranspiration are slightly overestimated, while transpiration and runoff are underestimated to about the same degree.

c. *Sensitivities*

Sensitivities of annual totals of model variables to fraction of vegetation (f_v), soil matric potential (H),

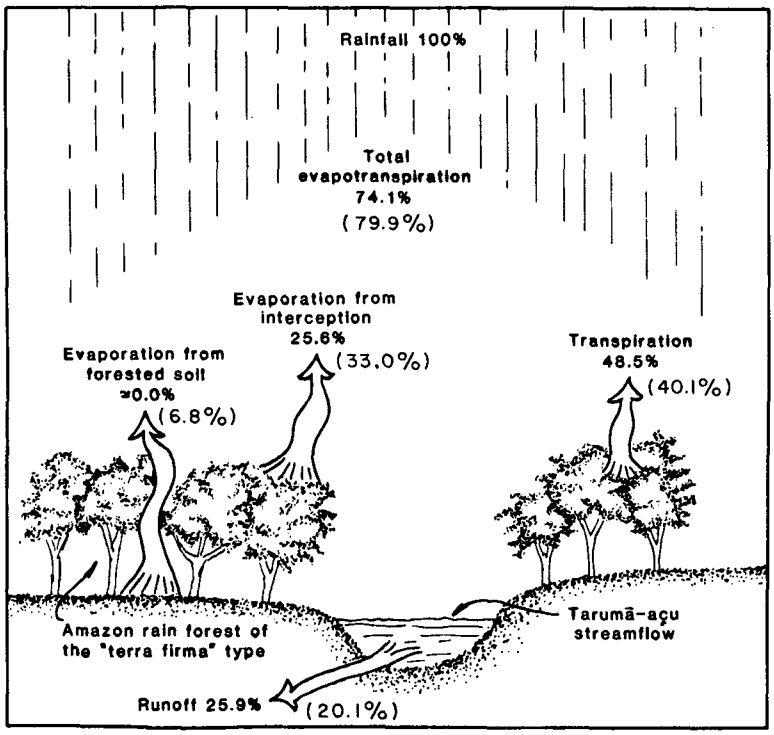

FIG. 17. Water balance from a study of a model basin near Manaus (Salati and Vose 1984). Water balance values for Brazilian rainforest from ground hydrology model are in parentheses.

soil hydraulic conductivity (K), and canopy resistance (R_c) were determined by running the model at equilibrium soil moisture first with specified values of the characteristics and then with a small change in these values. The sensitivity of y with respect to x is defined as

$$\left(\frac{x}{y}\right)\left(\frac{dy}{dx}\right), \tag{36}$$

where x is the prescribed characteristic and y is the dependent variable. Results are shown in Table 3. In general, hydrological variables are more sensitive to f_v than to canopy resistance and soil properties. Changes in f_v affect levels of both transpiration and evaporation from bare soil and this generally leads to significant changes in the water content of the soil layers. Thus, evapotranspiration components and runoff are sensitive to small changes in f_v. In contrast, hydrological variables are less sensitive to a 10% change in canopy resistance, since this affects only one component of evaporation, transpiration, and since canopy resistance acts in series with boundary layer resistance. Hydrological variables, except for θ and underground runoff, are not very sensitive to small changes in soil water potential and hydraulic conductivity.

5. Conclusions

Land–surface processes and their interactions with the atmosphere and climate are believed to be a major area of needed improvement in GCMs. It has not yet been fully determined what level of complexity is needed to provide sufficiently realistic hydrology for climate modeling, both in terms of parameterizations of land–surface processes and prescription of land–surface characteristics. The ground hydrology model described in this paper should contribute to more realistic and accurate global climate models, since processes are modeled on the basis of underlying physical principles yet are still simple enough to be compatible with other parts of a GCM. The use of composite soil and vegetation characteristics has been justified by comparison with high resolution results in four regions. Hydrological variables in the model are sensitive to the fraction of land surface covered by vegetation. Continued tests with this model, both off-line and coupled to a GCM, should help to determine the optimum level of detail for describing land–surface processes in global climate models.

TABLE 3. Sensitivities of annual hydrological variables[a] to fraction of land surface covered by vegetation, water potential, hydraulic conductivity, and canopy resistance.

	ET	Trans	Evap	EWC	LH	SH	UR	Theta
				Sahel				
FV (1% inc.)	−0.08	3.03	−0.47	1.01	−0.04	0.07	−14.38	0.42
H (10% inc.)	0.04	−2.0	0.29	0.00	0.04	−0.07	−0.05	−0.09
K (10% inc.)	0.02	−0.69	0.10	0.00	0.01	−0.02	1.06	−0.23
RC (10% inc.)	−0.01	−0.27	0.03	0.00	−0.01	−0.01	0.22	0.02
				Brazil				
FV (1% inc.)	−0.68	1.01	−18.97	0.99	−0.71	1.92	−2.67	0.24
H (10% inc.)	0.00	0.00	0.00	0.00	0.00	0.00	0.00	0.03
K (10% inc.)	−0.01	−0.01	0.00	0.00	−0.01	−0.01	0.08	−0.17
RC (10% inc.)	−0.20	−0.41	0.00	0.00	−0.20	−0.57	0.81	0.07
				Sahara				
FV (1% inc.)	0.11	0.00	1.05	1*	0.07	−0.01	−0.27	0.04
H (10% inc.)	0.04	0.00	0.04	0.00	0.04	−0.01	−1.92	−0.23
K (10% inc.)	0.04	0.00	0.04	0.00	0.05	−0.01	0.32	−0.20
RC (10% inc.)	0.00	0.00	0.00	0.00	0.00	0.00	0.00	0.00
				India				
FV (1% inc.)	−0.95	1.04	−3.00	1.01	−1.03	1.73	2.81	0.28
H (10% inc.)	−0.01	−0.03	0.00	0.00	−0.01	0.02	0.00	0.01
K (10% inc.)	−0.01	−0.03	0.00	0.00	−0.02	0.02	0.04	−0.21
RC (10% inc.)	−0.19	−0.50	0.00	0.00	−0.20	0.34	0.57	0.06

* $\frac{\Delta EWC}{\Delta FV} = \frac{-0.1774}{0.01} = -17.74$

[a] Evapotranspiration, transpiration, evaporation, evaporation of water stored on canopy, latent heat, sensible heat, underground runoff, mean volumetric moisture content (theta).

Acknowledgments. We thank Dr. L. Zobler for the soil file, profiles, and hydraulic properties, Dr. D. Hillel for his advice on soil water movement, Dr. K. Prentice for the seasonal LAI values, and B. Staub for the plotting programs. Drs. R. Gurney, W. J. Shuttleworth, D. Rind, G. Russell, and R. Dickinson reviewed the manuscript and provided helpful suggestions. L. Del Valle and J. Mendoza did the graphics. This work is supported by the Research and Development Branch of the Environmental Protection Agency.

APPENDIX A

Derivation of Water Table Depth Equation

The derivation is performed in two parts. First, static conditions are assumed (i.e., no water flow). Then this condition is relaxed and a general formula, taking fluxes into account, is derived. The general formula (which reduces to the static formula when the fluxes are zero) is used in the soil model.

1. Static case

Given a vertical column of soil with an impermeable layer at the bottom, consider the distribution of water if there are no fluxes. There may be a region at the bottom which is saturated. The top of this region is defined as the water table, and is at a depth z_w. The matric potential below z_w is zero. If z_w is taken as the reference height for the gravitational potential, then the total potential at z_w is zero. Because the flux is zero, the total potential at any point above the water table must also be zero:

$$h(\theta(z)) = z_w - z \quad \text{for} \quad z > z_w,$$
$$h(\theta(z)) = 0 \quad \text{for} \quad z < z_w. \tag{A1}$$

Suppose we have a model layer which is the first nonsaturated layer above the impermeable surface. Then, in general, this layer must contain the water table. Let z_1 be the lower boundary of this layer, and z_2 the upper boundary as shown in Fig. 5. Then,

$$z_1 < z_w < z_2. \tag{A2}$$

The average matric potential in this layer is

$$\bar{h}(z_1, z_2) = \int_{z_1}^{z_2} h(\theta(z))dz \Big/ (z_2 - z_1). \tag{A3}$$

Substituting (A1) into (A3), making use of (A2), we have

$$\bar{h}(z_1, z_2) = \int_{z_w}^{z_2} (z_w - z)dz \Big/ (z_2 - z_1). \tag{A4}$$

Integrating, we have

$$\bar{h}(z_1, z_2) = -\frac{1}{2}(z_w - z_2)^2/(z_2 - z_1). \tag{A5}$$

This expression can now be solved for z_w,

$$z_w = z_2 - (-2\bar{h}(z_1, z_2)(z_2 - z_1))^{1/2}. \tag{A6}$$

Since $\bar{h}(z_1, z_2)$ can be interpreted as being the same quantity as the soil model's value of h for the given layer, z_w can be calculated as a model diagnostic.

Equation (A6) should only be used when the fluxes are zero. It fails in the general case because (A1) does not hold if a flux is present.

2. General case

Let us consider the same conditions as case (1) except that a nonzero flux is permitted. The flux at any depth z is given by Darcy's law as

$$F(z) = -K(\theta(z))(1 + dh(\theta(z))/dz). \tag{A7}$$

This can be rewritten in the form

$$dh = -(F/k + 1)dz, \tag{A8}$$

where the arguments have been omitted to simplify the notation. As in case (1), $h = 0$ below the water table so that (A7) and (A8) are only valid for $z > z_w$. The matric potential at any level above the water table can be expressed as

$$\int_{z_w}^{z} dh = -\int_{z_w}^{z} (F(z^*)/K(\theta(z^*)) + 1)dz^*. \tag{A9}$$

Integrating, we obtain an equation that replaces (A1) when $z > z_w$,

$$h(\theta(z)) = (z_w - z) - \int_{z_w}^{z} (F/K)dz^*. \tag{A10}$$

The average matric potential in the layer is obtained by applying (A2) to (A10):

$$\bar{h}(z_1, z_2) = -\frac{1}{2}(z_w - z_2)^2/(z_2 - z_1) - \int_{z_w}^{z_2}\int_{z_w}^{z} (F/K)dz^*dz/(z_2 - z_1), \tag{A11}$$

where we have assumed that $F = 0$ below the water table. Let us define a dimensionless function q for a given flow as

$$q(z_w, z_2) = 2\int_{z_w}^{z_2}\int_{z_w}^{z} (F/K)dz^*dz/(z_w - z_2)^2. \tag{A12}$$

Equation (A11) can be combined with (A12) to yield

$$\bar{h}(z_1, z_2) = -\frac{1}{2}(q(z_w, z_2) + 1)(z_w - z_2)^2/(z_2 - z_1). \tag{A13}$$

Rearranging, we have

$$z_w = z_2 - (-2\bar{h}(z_1, z_2)(z_2 - z_1)/(q(z_w, z_2) + 1))^{1/2}. \tag{A14}$$

This is not strictly a solution for z_w because the right-hand side depends on z_w through q. Unfortunately, q depends on the details of the flow and is therefore not a well-defined quantity for a numerical solution. However, a rough estimate for q can be made as follows. First, expand $h(z)$ in a Taylor series about z_w:

$$h(z) = h(z_w) + h'(z_w)(z - z_w) + \frac{1}{2}h''(z_w)(z - z_w)^2 + \cdots. \tag{A15}$$

As always, we will take $h(z_w)$ to be zero. If we now assume that $h'(z_w)$ is not zero, then for z sufficiently close to z_w we can approximate h as

$$h(z) \approx h'(z_w)(z - z_w). \tag{A16}$$

Substituting (A16) into (A7) we obtain an approximate expression for the flux,

$$F(z) \approx -K(\theta(z))(1 + h'(z_w)). \tag{A17}$$

We can use equation (A17) in (A12) and write $q(z_w, z_2)$ as

$$q(z_w, z_2) = 2 \int_{z_w}^{z_2} \int_{z_w}^{z} -(1 + h'(z_w))dz^* dz/(z_w - z_2)^2. \quad \text{(A18)}$$

This can be integrated immediately as

$$q(z_w, z_2) \approx -(1 + h'(z_w)). \quad \text{(A19)}$$

The right-hand side of this equation can be estimated by applying (A17) at $z = z_2$, so that

$$q(z_w, z_2) \approx F(z_2)/K(\theta(z_2)). \quad \text{(A20)}$$

This enables q to be determined from known quantities, since both F and K must be available at the boundary $z = z_2$ in a numerical solution. Therefore (A20) combined with (A14) defines the level of the water table for a general numerical solution. Note that if the fluxes are zero, equation (A14) reduces to the static case solution (A6), because by (A20) q is equal to zero.

APPENDIX B

Symbols

C_D	drag coefficient
C_h	humidity transfer coefficient
c_p	specific heat of air at constant pressure, cal kg^{-1} K^{-1}
D	diffusivity, kg m^{-1} s^{-1}
D_1	diffusivity of the first soil layer, kg m^{-1} s^{-1}
E	actual evaporation from bare soil, kg m^{-2} s^{-1}
E_{max}	maximum evaporation from bare soil, kg m^{-2} s^{-1}
E_p	potential evaporation from bare soil, kg m^{-2} s^{-1}
E_{wc}	canopy evaporation, kg m^{-2} s^{-1}
ET	actual evapotranspiration, kg m^{-2} s^{-1}
ET_l	mean evapotranspiration from layer l, kg m^{-2} s^{-1}
ET_p	potential evaporation, kg m^{-2} s^{-1}
e_a	saturated vapor pressure at surface air temperature, N m^{-2}
e_d	saturated vapor pressure at dewpoint temperature, N m^{-2}
F	water flux, kg m^{-2} s^{-1}
F_l	flux between layers l and $l-1$, kg m^{-2} s^{-1}
F_l^α	flux evaluated at a time intermediate between the present time step and the next time step, kg m^{-2} s^{-1}
f_d	fraction of canopy which is dry
$f_r(l)$	fraction of roots present in soil layer
f_v	fraction of land covered (shaded) by vegetation
f_w	fraction of canopy which is wet
H_l	total potential (matric plus gravitational) of layer l, m
H_0	net heat at surface, W m^{-2}
H_w	wilting point, m
h	matric potential, m
h_1	matric potential in layer 1, m
$\bar{h}(z_1, z_2)$	average matric potential in layer where water table occurs, m
I_{max}	infiltration capacity, kg m^{-2} s^{-1}
J	mechanical equivalent of heat, J cal^{-1}
K	hydraulic conductivity, kg m^{-2} s^{-1}
K_l	hydraulic conductivity between layers l and $l-1$, kg m^{-2} s^{-1}
$\bar{K}_l$	mean conductivity in layer l, kg m^{-2} s^{-1}
L	number of layers in soil model
LAI	leaf area index
LAI_c	maximum value of LAI_e
LAI_e	effective leaf area index
l	layer in soil model
P_r	precipitation rate, kg m^{-2} s^{-1}
q	dimensionless flow from water table
R_a	boundary layer resistance for vapor transfer, s m^{-1}
R_c	canopy resistance of vegetation, s m^{-1}
R_n	net radiation, W m^{-2}
r_s	stomatal resistance, s m^{-1}
S	$\sin\chi$
T	actual transpiration, kg m^{-2} s^{-1}
T_l	actual transpiration from each soil layer, kg m^{-2} s^{-1}
T_s	surface air temperature, K
T_{unst}	unstressed transpiration, kg m^{-2} s^{-1}
VH	vegetation height, m
V_s	wind speed at surface plane, m s^{-1}
w_c	water stored on the canopy, sum of dew and intercepted precipitation, kg m^{-2}
w_l	quantity of water in layer l, kg m^{-2}
w_{sc}	canopy water storage capacity, kg m^{-2}
y	coordinate perpendicular to z in the uphill direction, m
ZD	zero plane displacement, m
Z_l	mean depth of layer l, m
ΔZ_l	thickness of layer l, m
ZO	surface roughness of vegetation, m
z	depth, or perpendicular distance below the surface, m
z_w	depth of water table, m
$\beta_w(l)$	soil moisture availability in layer l
γ	psychrometric constant, N m^{-2} K^{-1}
Δ	slope of saturated vapor pressure curve, N m^{-2} K^{-1}
δ	distance between streams, m
θ	volumetric moisture content
r_{sat}	water content at saturation, kg m^{-2}
λ	latent heat of vaporization, cal kg^{-1}
ρ	density of air, kg m^{-3}
χ	angle of soil surface from horizontal

REFERENCES

Aston, A. R., 1984: Evaporation from eucalypts growing in a weighing lysimeter: A test of the combination equations. *Agri. and For. Meteor.*, **31**, 241–249.

Bosen, J. F., 1960: A formula for approximation of saturation vapor pressure over water. *Mon. Wea. Rev.*, **88**(8), 275–276.

Brunt, D., 1952: *Physical and Dynamical Meteorology*, 2nd ed., University Press, Cambridge, 428 pp.

Carson, B. J., 1982: Current parameterizations of land-surface processes in atmospheric general circulation models. *Land Surface Processes in Atmospheric General Circulation Models*, P. S. Eagleson, Ed., Cambridge University Press.

Collinson, A. S., 1977: *Introduction to World Vegetation.* George Allen and Unwin.

Deardorff, J. W., 1978: Efficient prediction of ground surface temperature and moisture, with inclusion of a layer of vegetation. *J. Geophys. Res.*, **83**, 1889–1903.

Dickinson, R. E., 1984: Modeling evapotranspiration for three-dimensional global climate models. *Climate Processes and Climate Sensitivity*, J. E. Hansen and T. Takahashi, Eds., Amer. Geophys. Union, Washington DC, 58–72.

Epstein, E., 1973: Roots. *Sci. Amer.*, **228**(5), 48–58.

FAO-UNESCO, 1974: Soil Map of the World 1:5,000,000. UNESCO, Paris.

Fetcher, N., B. R. Strain and S. F. Oberbauer, 1983: Effects of light regime on the growth, leaf morphology, and water relations of seedlings of two species of tropical trees. *Oecologia*, **58**, 314–319.

Gardner, W. R., and D. Hillel, 1962: The relation of external evaporative conditions to the drying of soils. *J. Geophys. Res.*, **67**, 4319–4325.

Geiger, R., 1965: *The Climate Near the Ground.* Harvard University Press, 611 pp.

Hanks, R. J., and S. A. Bowers, 1962: Numerical solution of the moisture flow equation for infiltration into layered soils. *Soil Sci. Soc. Am. Proc.*, **26**, 530–534.

Hansen, J., G. Russell, D. Rind, P. Stone, A. Lacis, S. Lebedeff, R. Reudy and L. Travis, 1983: Efficient three-dimensional global models for climate studies, Models I and II. *Mon. Wea. Rev.*, **111**, 609–662.

Hillel, D., 1982: *Introduction to Soil Physics.* Academic Press, 364 pp.

Klinge, H., 1973: Root mass estimation in lowland tropical rain forests of central Amazonia, Brazil. I: Fine root masses of a pale yellow latosol and a giant humus podzol. *Trop. Ecol.*, **14**(1), 29–38.

Körner, C. H., J. A. Scheel and H. Bauer, 1979: Maximum leaf diffusive conductance in vascular plants. *Photosynthetica*, **3**, 45–82.

Kutschera, L., 1960: *Wurzelatlas* DLG-Verlags-GMBH.

Matthews, E., 1983: Global vegetation and land use: new high-resolution data bases for climate studies. *J. Climate Appl. Meteor.*, **22**, 474–487.

——, 1984: Vegetation, land-use and seasonal albedo data sets: documentation of archived data tape. NASA Tech. Memo. 86107, 20 pp.

Monteith, J. L., 1973: *Principles of Environmental Physics.* Edward Arnold, 236 pp.

——, 1981: Evaporation and surface temperature. *Quart. J. Roy. Meteor. Soc.*, **107**, 1–27.

Mualem, Y., 1976: A new model for predicting the hydraulic conductivity of unsaturated porous media. *Water Resour. Res.*, **12**, 513–522.

Odum, H. T., and R. F. Pigeon, 1970: Rain forest structure and mineral-cycling homeostasis. *A Tropical Rain Forest.* A study of irradiation and Ecology at El Verde, Puerto Rico. U.S. Atomic Energy Commission, Washington, DC: H-3–H-57.

Penman, H. L., 1948: Natural evaporation from open water, bare soil, and grass. *Proc. Roy. Soc. London*, **A193**, 120–145.

Rutter, A. J., 1975: The hydrological cycle in vegetation. *Vegetation and the Atmosphere.* Vol. 1. J. L. Monteith (Ed). Academic Press. 111–154.

Schulze, E.-D., 1982: Plant life forms and their carbon, water, and nutrient relations. *Physiological Plant Ecology II*, O. L. Lange, P. S. Nobel, C. B. Osmond, and H. Ziegler, Eds. Springer-Verlag, 615–676.

Sellers, P. J., Y. Mintz, Y. C. Sud and A. Dalcher, 1986: A simple biosphere (SiB) for use within General Circulation Models. *J. Atmos. Sci.*, **43**(6), 505–531.

Shuttleworth, W. J., J. H. C. Gash, C. R. Lloyd, C. J. Moore, J. Roberts, A. De O. Marques Filho, G. Fisch, V. De Paula Silva Filho, L. C. B. Molion, L. D. De Abreu Sa, J. C. A. Nobre, O. M. R. Cobral, S. R. Patel and J. De Moraes, 1984: Eddy correlation measurements of energy partition for Amazonian forest. *Quart. J. Roy. Meteor. Soc.*, **110**, 1143–1162.

Thornthwaite, C. W., and J. R. Mather, 1962: Average Climate Water Balance Data of the Continents. Part I. Africa: Publications in climatology, Vol. XV, No. 2, Laboratory of Climatology, Centerton, NJ.

UNESCO, 1973: *International Classification and Mapping of Vegetation.* Paris, UNESCO, 93 pp.

Wang, F. C., and V. Lakshminarayana, 1968: Mathematical simulation of water movement through unsaturated nonhomogeneous soil. *Soil Sci. Soc. Am. Proc.*, **32**, 329–334.

Zobler, L., 1986: A world soil file for global climate modeling. NASA Tech. Memo. 87802.